J Intell Robot Syst (2017) 87:247–263
DOI 10.1007/s10846-017-0477-x

Design and Implementation of a Multi Sensor Based Brain Computer Interface for a Robotic Wheelchair

Gurkan Kucukyildiz · Hasan Ocak · Suat Karakaya · Omer Sayli

Received: 13 June 2016 / Accepted: 8 January 2017 / Published online: 31 January 2017

Abstract In this study, design and implementation of a multi sensor based brain computer interface for disabled and/or elderly people is proposed. Developed system consists of a wheelchair, a high-power motor controller card, a Kinect camera, electromyogram (EMG) and electroencephalogram (EEG) sensors and a computer. The Kinect sensor is installed on the system to provide safe navigation for the system. Depth frames, captured by the Kinect's infra-red (IR) camera, are processed with a custom image processing algorithm in order to detect obstacles around the wheelchair. A Consumer grade EMG device (Thalmic Labs) was used to obtain eight channels of EMG data. Four different hand movements: Fist, release, waving hand left and right are used for EMG based control of the robotic wheelchair. EMG data is first classified using artificial neural network (ANN), support vector machines and random forest schemes. The class is then decided by a rule-based scheme constructed on the individual outputs of the three classifiers. EEG based control is adopted as an alternative controller for the developed robotic wheelchair. A wireless 14-channels EEG sensor (Emotiv Epoch) is used to acquire real time EEG data. Three different cognitive tasks: Relaxing, math problem solving, text reading are defined for the EEG based control of the system. Subjects were asked to accomplish the relative cognitive task in order to control the wheelchair. During experiments, all subjects were able to control the robotic wheelchair by hand movements and track a pre-determined route with a reasonable accuracy. The results for the EEG based control of the robotic wheelchair are promising though vary depending on user experience.

Keywords Robotic wheelchair · EEG · EMG · Navigation · Brain-computer interface

1 Introduction

Disabled people, who suffer from amyotrophic lateral sclerosis (ALS) or tetraplegia, can lose their motor ability functions. Consequently, such people may not easily control conventional wheelchairs. Therefore, researchers have an interest in converting wheelchairs to robotic forms by using various techniques [1, 2]. Kim and his team developed a tongue-driven system to control a powered wheelchair [3]. The authors developed a headset, which consists of magnetic sensor

H. Ocak (✉) · G. Kucukyildiz · S. Karakaya
Department of Mechatronics Engineering, Umuttepe Campus, Kocaeli University, 41380 Kocaeli Turkey
e-mail: hocak@kocaeli.edu.tr

G. Kucukyildiz
e-mail: gurkan.kucukyildiz@kocaeli.edu.tr

S. Karakaya
e-mail: suat.karakaya@kocaeli.edu.tr

O. Sayli
e-mail: omer.sayli@hotmail.com

boards and a control unit. A piercing is placed on the tongue of each subject. The magnetic sensor on the headset senses the motion of the tongue. Six different tongue movements were defined in the study: up, down, left, right, neutral, left select and right select. The authors applied k-nearest neighbor (KNN), Mahalonobis and Euclidian distance based methods for classifying the tongue movements. The tongue movement was determined based on majority of voting. Carlson and Jose developed a brain-computer interface (BCI) based robotic wheelchair system [4]. The proposed system consists of encoders for each wheel, a joystick, webcams, ultrasonic sensors and a power distribution unit. They developed a computer vision based obstacle detection algorithm with stereo vision and ultrasonic sensors. A 16-channel EEG system having a sample rate of 512 Hz was utilized in the study. In the pre-processing step, a Laplacian filter was applied to EEG data to improve the signal to noise ratio (SNR). Power spectral densities (PSD) of commonly used EEG bands were selected as features for classifying EEG signals. Since EEG could vary among people, the authors preferred to use subject-dependent features in their classification scheme. They used canonical variate analysis to select subject-specific features to maximize the classification performance. Kim and his team developed a bio-signal based robotic wheelchair [5]. The authors developed a BCI system based on EMG artifact detection in EEG signals. Four cognitive tasks were defined to control the system: clenching of the teeth, blinking of the eyes, wrinkling of the forehead and frowning. Linear predictive coding (LPC) coefficients were used as features in a hidden Markov model (HMM) based classification scheme. Grasse and his team developed an assisted navigation system based on path recognition [6]. The authors used simultaneous localization and mapping (SLAM) method for the localization of the wheelchair. Particle filtering was used for path recognition. Four different types of paths were tracked by the subjects. Noda and his team proposed a mechatronics vision for smart robotic wheelchairs [7]. They used omnidirectional wheels to increase the maneuverability of the wheelchair. The proposed system could sense the environment by means of ultrasonic and infrared sensors installed on the system. In addition, a 6 axis force sensor based haptic was also installed on the system. Gulrez and Tongetti developed a body-machine interface to control a simulated robotic wheelchair system in the 3D virtual Matlab environment [8]. The authors developed a sensor shirt, which includes 52 piezoresistive sensors, to detect the local movements of the users' upper body. They used principal component analysis (PCA) to reduce the dimensions of 52 signal data space obtained from the sensor shirt. The developed system was tested by three subjects over six months. The position errors of each subject in path tracking task were seen to decrease in time by training.

Wearable technology devices consist of sensors, which could detect the movements in the muscles and convert them to the electrical signals. In this study, commercial wearable devices based robotic wheelchair was developed. The developed system consists of a wheelchair, a computer, a motor controller, a Kinect sensor, an EMG armband and a portable wireless EEG device. The devices used on the system were selected as low cost commercial devices. One can control the proposed robotic wheelchair system by means of either an EMG armband or an EEG headset. Kinect based image processing algorithm was developed in order to provide safe navigation for the system. The proposed system was tested on four (2 experienced, 2 unexperienced) 20-30 aged healthy subjects. To test the real-time performance of the system, subjects were asked to track three different routes: sinusoidal, circular, rectangular. During the route tracking experiments, exact position measurements were taken with a laser meter. In separate two experiments, each subject was asked to track the routes controlling the wheelchair using either EMG or EEG. It was observed that, subjects could successfully track the three different routes with EMG based control. The route tracking performance for the EEG based control was promising, though depended on user experience and environmental conditions.

2 Technical Background

2.1 Support Vector Machines (SVM)

SVM is one of the statistical learning theory based supervised machine learning methods. Having better generalization performance and robustness compared to classical learning procedures, SVM has successfully been applied to various fields in recent years [9–11]. The main goal of an SVM classifier is to find the optimum hyper plane that separates two classes

from each other. The hyper plane, which has the highest margin between the two classes, is called as the optimum hyper plane. The illustration of SVM based binary classification and the optimum hyper plane is depicted in Fig. 1.

The points that are closest to the separating hyper plane are referred to as support vectors. Since the hyper plane lies on the middle of support vectors, the Euclidian distance between two support vectors, also known as the SVMs margin, can be calculated as $2/\|\boldsymbol{w}\|$ by simple vector geometry. The orientation of the optimal hyperplane is set such that this margin is maximized. If the training data is fully linearly separable, the optimization problem can be stated as,

$$\min \frac{1}{2}\|w\|^2 \text{ s.t. } y_i(w\varphi(x_i)+b) \geq 1 \tag{1}$$

where **w** is the weight vector, b is the bias and φ is the SVM' s kernel function. In non-linear optimization problems, the optimal solution must respect the Kuhn-Tucker conditions [12] and can be determined by minimizing the Lagrangian function given by,

$$L_p(w,b,\alpha) = \frac{1}{2}\|w\|^2 - \sum_{i=1}^{N}\alpha_i\left[y_i(w\varphi(x_i))+b\right] + \sum_{i=1}^{N}\alpha_i \tag{2}$$

where α is a vector of Lagrange multipliers. The Lagrange multipliers, which have values higher than 0, are referred to as support vectors. In this study, the kernel function, φ, for the SVM classifier was selected as the quadratic function.

2.2 Random Forests (RF)

Although the decision tree technique was originally proposed by Morgan and Sonquiest in 1963, the technique only started to be used frequently for classification applications after a study published by Breiman in 1984 [13, 14]. In a decision tree, training data is separated into two groups according to features till pure class samples are obtained.

Figure 2 illustrates the principle behind the random forest classification algorithm. Initially, the training data is split into left and right nodes based on a threshold applied to the first feature. The threshold is selected to minimize the residual sum of squares, called as the regression criteria, given below.

$$R_{ss} = \sum_{left}(y_i - y_l)^2 + \sum_{right}(y_i - y_r)^2 \tag{3}$$

$y_i$is the value for the corresponding feature for the i-th sample, y_l and y_r are the mean values for the feature given the samples assigned to the left and the right nodes, respectively. This splitting procedure is applied to all nodes repeatedly using the next feature at each level of the decision tree. Splitting procedure is not applied to nodes for which pure class samples are obtained. Data separation is accomplished for the other nodes until pure class samples are obtained for all the end nodes in the binary decision tree. The Gini index is defined by,

$$Gini = N_l\sum_{k=1}^{K}p_{kl}(1-p_{kl}) + Nr\sum_{k=1}^{M}p_{kr}(1-p_{kr}) \tag{4}$$

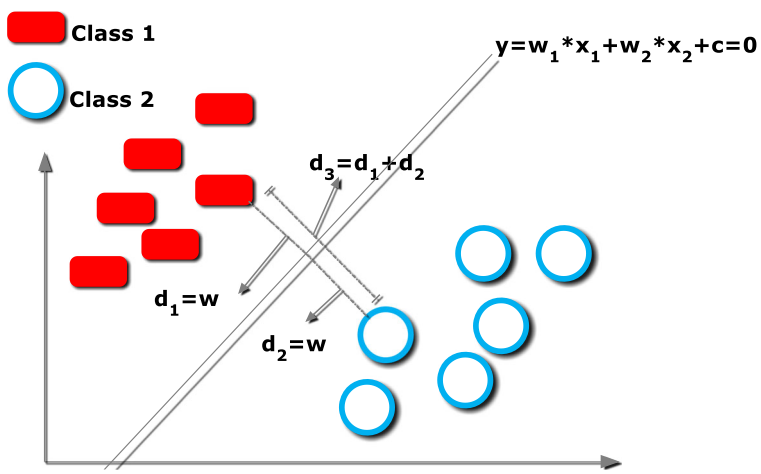

Fig. 1 SVM based binary classification

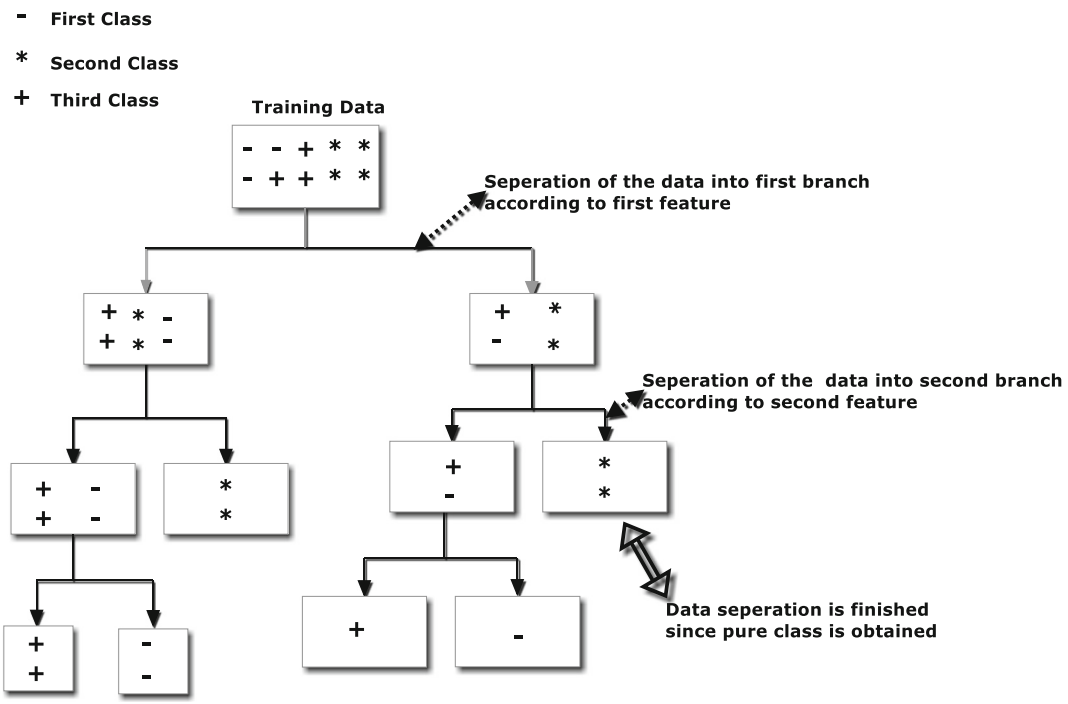

Fig. 2 Random Forest based classification

N_l and N_r are the total number of samples assigned to the left and the right nodes respectively. p_{kl} and p_{kr} are the proportions of *k-th* class in the left and right nodes. Each time the data is split into left and right nodes based on a feature, the Gini index for the two nodes is less than the one of the parent node. Adding up the Gini decreases for each individual feature over all trees in the forest gives a measure for feature importance that is consistent with the permutation importance measure.

Since the classification accuracy of a decision tree is highly dependent on the training data, in a random forest structure several decision trees are constructed from random subsets of the training data. The output of the random forest classifier is computed as the average outputs of the individual trees, that is defined by,

$$RO = \frac{1}{M}\sum_{i=1}^{M} Ti \tag{5}$$

where M is the number of the grown trees, and T_i is the output of i-th tree.

2.3 Approximate Entropy (ApEn)

ApEn is a time-domain based feature which measures the predictability of a signal. It is widely used for EEG analysis [15]. Unpredictable signals have higher ApEn values than predictable signals. Steps for calculating ApEn of an N point time series y_i, i =1,..., N is given below. First, the state vectors in the embedded space are defined as,

$$x_i = \left\{ y_i, y_{i+\tau}, y_{i+2\tau} \ldots\ldots, y_{i+(m-1)\tau} \right\}, \quad 1 \le i \le N-(m-1)\tau \tag{6}$$

where m represents the embedding dimension and τ represents the time delay. For each i, we define

$$C_i^m(r) = \frac{1}{N-(m-1)\tau} \sum_{j=1}^{N-(m-1)\tau} \theta(r - d(x_i, x_j)) \tag{7}$$

θ is the standard Heavyside function and is defined as,

$$\theta(x) = \begin{cases} 1, & x \ge 0 \\ 0, & \text{otherwise} \end{cases} \tag{8}$$

r is the vector comparison distance that is used to compare state vector in the embedding space and $d(x_i, x_j)$ is a distance measure defined as,

$$d(x_i, x_j) = \max_{k=1,2....m} (\left|y_{i+(k-1)\tau} - y_{j+(k-1)\tau}\right|) \quad (9)$$

$\varphi^m(r)$ is be defined as,

$$\varphi^m(r) = \frac{1}{N-(m-1)\tau} \sum_{i=1} \log C_i^m(r) \quad (10)$$

Finally, ApEn of a signal for fixed m, r, τ can be calculated as,

$$ApEn = \varphi^m(r) - \varphi^{m+1}(r) \quad (11)$$

In this study, the embedding dimension (m), vector comparison distance (r) and time delay (τ) were set to 2, 0.15 times the standard deviation of the data and 1, respectively based on suggestions given in [15].

3 Experimental Setup and System Architecture

In this study, design and navigation of a robotic wheelchair system is proposed. A powered wheelchair system was purchased and modified through the main concerns of the study. An industrial computer was placed on the robotic wheelchair to run the developed algorithms. The wheelchair's built-in DC motor controller was replaced with the custom ones designed and manufactured by the authors. Users have an option to control the system through EMG or EEG signals. A wireless consumer grade EMG armband (Thalmic Labs Myo-Armband) was used for the EMG based control of the system. For the EEG based control on the other hand, a 14 channel (AF3, F7, F3, FC5, T7, P7, O1, O2, P8, T8, FC6, F4, F8, AF4) Emotiv EEG device was used. Kinect based image processing algorithm was employed to ensure collision-free navigation. The general system architecture is given in Fig. 3.

The armband consists of eight EMG sensors, a gyroscope, an accelerometer and a magnetometer. The device communicates with a computer via Bluetooth. Developers can access raw EMG and gyro data using the software development kit distributed by Thalmic Labs [16, 17]. In this study, raw data acquired from the EMG armband was streamed to MATLAB environment in real time through a Bluetooth connection with 115200 baud rate. Subjects were required to undergo training prior to using the robotic wheelchair system. In the training phase, they were asked to accomplish four different hand movements: making a fist, hand release, waving hand left and right. The sampling period for the Myo-Armband was set to 1 kHz for each channel. Fifty milliseconds of data (50 measurements) were obtained from each channel in real time to be classified into one of the pre-defined hand movements.

A commercial Emotive headset was used for the EEG based control of the system. The sampling rate and the resolution for the device were set to 128 Hz and 14 bits by the manufacturer, respectively. Emotive headset has serious advantages compared to the conventional EEG devices such as portability, having wireless connection and no expert requirement for usage [18–20]. On the other hand, the sensors of the Emotive device can easily oxidize which could affect the EEG data quality. Each sensor should be wetted with a saline solution to enhance conductivity before each usage. Sensors should be cleaned with alcohol after each usage in order to prevent the oxidation. Developers can record raw EEG data in '.edf' format using the test-bench program which is installed automatically with Emotiv Research Edition SDK. Similar to EMG based control the subjects were required to undergo training prior to using the robotic wheelchair system. In the training phase, they were asked to accomplish three different cognitive tasks: relaxing, math problem solving and text reading. Real time EEG data was obtained through a third party application developed by the authors in Visual Studio environment. EEG data was then streamed from the developed program to MATLAB via a UDP connection.

4 Methods

4.1 Vision Based Safe Navigation

Providing safe navigation is very crucial in robotic wheelchair applications. Researchers used various techniques such as ultrasonic sensors, light detection and ranging sensor (LIDAR) to ensure safe navigation [3]. In this study, an image processing based safe navigation scheme was developed. Although Kinect was initially developed by Microsoft in 2010 for gaming technology, its content has increased the researchers' interest on Kinect [21–23]. Kinect can construct depth images by using IR projector. In this study Kinect's

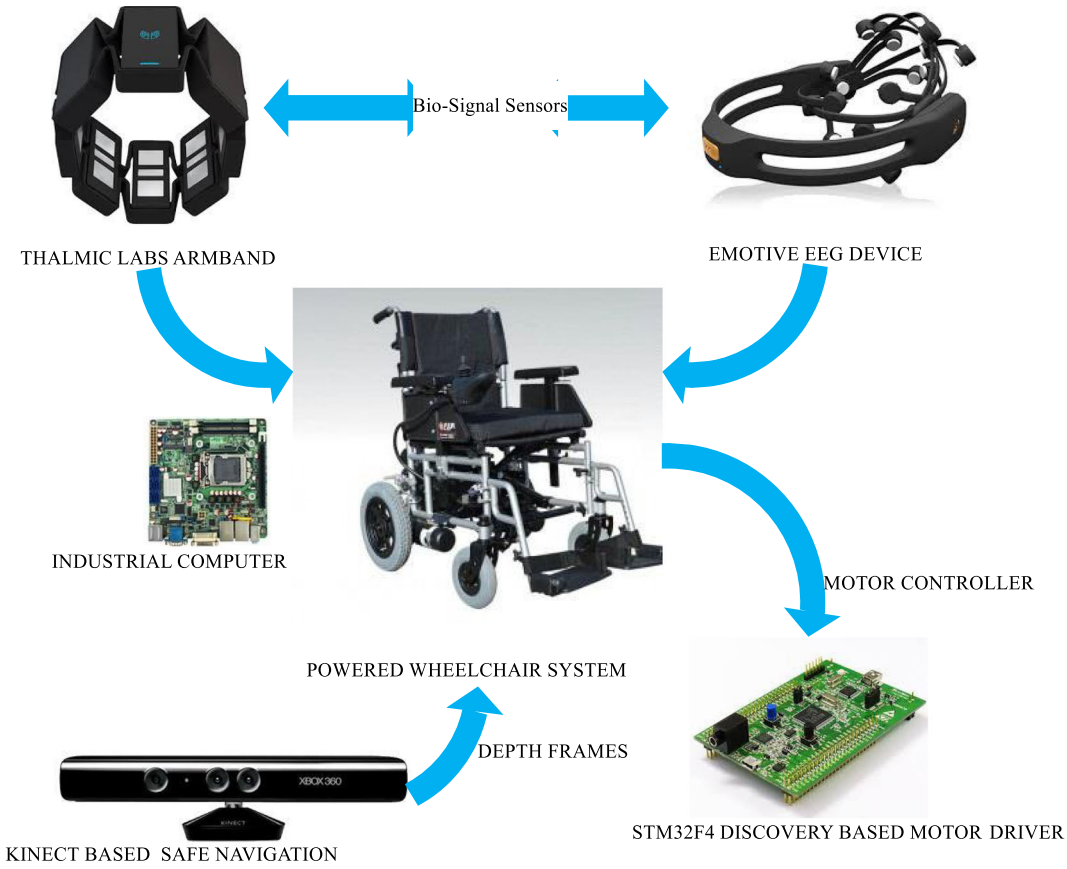

Fig. 3 The system architecture

depth camera was used to provide safe navigation for the system. Depth images were obtained and processed by the developed image processing algorithm. Prior to executing a command received from either the EMG or EEG based controller, the system checks the environment to avoid any collusion. If an obstacle is detected by the developed image processing algorithm, the safe navigation routine overwrites all other commands and the wheelchair is stopped. As illustrated in Fig. 4, Kinect's field of view is highly related with the mounting angle between Kinect's line of sight and the workspace floor. When the mounting angle is very small, the depth camera is unable to record any data on the floor surface. On the other hand, if mounting angle is very large the depth camera records only a limited area around the sit area of the wheelchair. The x-y plane of the Kinect's coordinate system and the floor plane are not parallel due to mounting angle. Therefore, it is necessary to make a coordinate transformation so that the x-y planes of the two coordinate systems are parallel. Following this transformation, all points on the floor should have the same depth value. To make this transformation, Kinect's coordinate system should be rotated with respect to x and y axes by using camera calibration.

Camera calibration is a major problem in image processing applications [24–26]. For calibrating a given camera, intrinsic and extrinsic matrices should be calculated. The intrinsic matrix depends on the camera's internal parameters such as focal length (f), principal point (c_x, c_y), pixel width (s_x) and pixel height (s_y). The intrinsic matrix, $\mathbf{M}$, of a camera is given in Eq. 11.

$$\mathbf{M}_{int} = \begin{bmatrix} -\frac{f}{s_x} & 0 & -c_x \\ 0 & -\frac{f}{s_y} & -c_y \\ 0 & 0 & 1 \end{bmatrix} \tag{12}$$

In this study, internal parameters of Kinect were obtained by using Kinect SDK. The parameters are

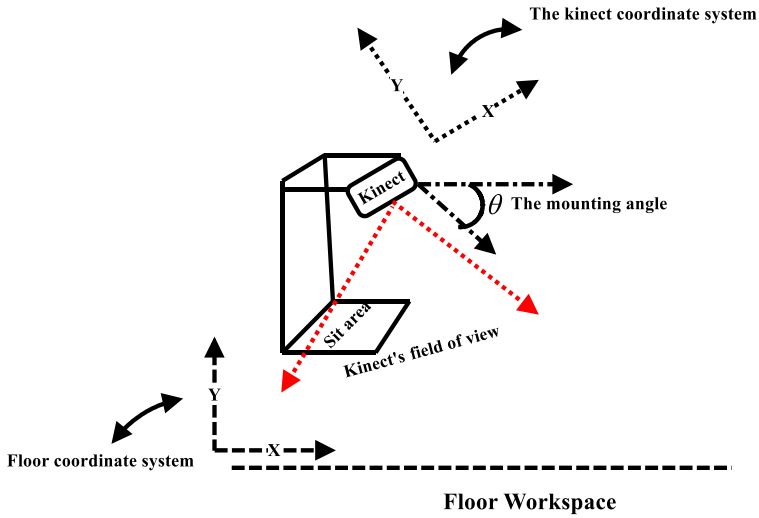

Fig. 4 The Kinect's placement

given in Table 1. Real world coordinates of a pixel can be calculated using Eq. 12.

$$\begin{bmatrix} \frac{x_k}{z_k} \\ \frac{y_k}{z_k} \\ 1 \end{bmatrix} = \mathbf{M}^{-1} \begin{bmatrix} i \\ j \\ 1 \end{bmatrix} \tag{13}$$

The Extrinsic matrix on the other hand depends on the camera placement. The depth value of a point on the floor as measured by Kinect varies depending on the location due to the mounting angle between the Kinect's line of sight and the workspace floor. Therefore Kinect's coordinate system should be rotated with respect to x and y axes to make a coordinate transformation. Rotation matrices around the x and y axes ($\mathbf{R}_x$, $\mathbf{R}_y$) are given in Eq. 13.

$$\mathbf{R}_x = \begin{bmatrix} 1 & 0 & 0 \\ 0 & cos(\theta) & -sin(\theta) \\ 0 & sin(\theta) & cos(\theta) \end{bmatrix},$$
$$\mathbf{R_y} = \begin{bmatrix} cos(\phi) & 0 & sin(\phi) \\ 0 & 1 & 0 \\ -sin(\phi) & 0 & cos(\phi) \end{bmatrix} \tag{14}$$

Table 1 Kinect parameters

Parameter	Value
f/s_x	591.040
f/s_y	594.21
c_x	242.73
c_y	339.30

Combined rotation matrix ($\mathbf{R} = \mathbf{R}_x\mathbf{R}_y$) is then given in Eq. 14. $\mathbf{R}_z$ is neglected since rotation around z-axis does not affect the depth measurements.

$$\mathbf{R} = \begin{bmatrix} \cos(\phi) & 0 & \sin(\phi) \\ \sin(\theta)\sin(\phi) & \cos(\theta) & -\sin(\theta)\cos(\phi) \\ -\cos(\theta)\sin(\phi) & \sin(\theta) & \cos(\theta)\cos(\phi) \end{bmatrix} \tag{15}$$

A point in Kinect coordinate system $p_k = [x_k\ y_k\ z_k]$ can be transformed to a corresponding point in the new coordinate system parallel to x-y plane of the workspace floor $p_m = [x_m\ y_m\ z_m]$ with $\mathbf{R}$ by Eq. 15.

$$\mathbf{p}_\mathrm{m} = \mathbf{R}\mathbf{p}_\mathbf{k} \tag{16}$$

Equation 15 can be rewritten as

$$\begin{aligned} x_m &= r_{11}x_k + r_{12}y_k + r_{13}z_k \\ y_m &= r_{21}x_k + r_{22}y_k + r_{23}z_k \\ z_m &= r_{31}x_k + r_{32}y_k + r_{33}z_k = d_m \end{aligned} \tag{17}$$

where r_{ij} is the i-th row and the j-th column element of $\mathbf{R}$. The depth value d_m must be constant for any point on the workspace floor. The third row of Eq. 16 can be rewritten as follows,

$$\mathbf{r}_3^T\,\mathbf{p}_m = d_m \tag{18}$$

where $\mathbf{r}_3$ is equal to the third row of the rotation matrix $\mathbf{R}$ and d_m is equal to the depth value of the workspace floor. All the points on the floor plane must satisfy Eq. 17. To solve for $\mathbf{r}_3$ and d_m, N points were taken on

the floor. The system of N equations was then written in matrix form as follows;

$$\begin{bmatrix} \mathbf{p}_{k1}^T & -1 \\ \mathbf{p}_{k2}^T & -1 \\ \mathbf{p}_{k3}^T & -1 \\ . & . \\ . & . \\ \mathbf{p}_{kN}^T & -1 \end{bmatrix} \begin{bmatrix} \mathbf{r}_3^T \\ d_m \end{bmatrix} = \mathbf{0} \tag{19}$$

Equation 18 can be expressed as $\mathbf{Ax} = \mathbf{0}$ format, where;

$$A = \begin{bmatrix} p_{k1}^T & -1 \\ p_{k2}^T & -1 \\ p_{k3}^T & -1 \\ . & . \\ . & . \\ p_{kN}^T & -1 \end{bmatrix} \text{ and } x = \begin{bmatrix} r_3^T \\ d_m \end{bmatrix} \tag{20}$$

Figure 5 shows an original depth map acquired from the Kinect sensor and the corrected depth map computed based on Equation 16. In the original depth map, the depth values of points on the workspace floor vary with the distance to wheelchair. On the other hand, the depth values of points on the workspace floor are approximately the same for the corrected depth image.

In the initial stage of the collision avoidance module, the background depth image is obtained by averaging the first acquired twenty images at the initialization of the system. Averaging is performed to reduce the amount of noise present in depth measurements. Images are captured from Kinect per 3.3 ms (30 fps) and when an image is captured, difference of the current captured image and the background image is calculated to be the foreground image. If the number of foreground pixels exceeds a pre-determined threshold, obstacle control is triggered. Since the presence of an obstacle around the wheelchair would reduce the depth values of the corresponding pixels with respect to Kinect sensor, a pixel is assumed to be part of an obstacle if the difference between its current and background values is higher than a threshold. Pixels located within the close vicinity of the sitting area are neglected since any motion in this region would mean the movement of the subject operating the wheelchair. A black and white (BW) image is constructed with the detected foreground pixels. Morphological opening is applied to the image for noise removal. Morphological closing and region filling is then applied to fill the gaps and holes. After these morphological operations, connected components algorithm is used to segment the image. A sample background image and resulting foreground image after morphological operations are given in Fig. 6.

5 Bio-Signal based control of Robotic Wheelchair

In the developed robotic wheelchair system, users are given the option to control the wheelchair through either the EMG armband or the Emotiv EEG headset. Four pre-defined tasks (making a fist, hand release, waving hand left and right) are used in EMG based control. The wheelchair is steered to the left, right and

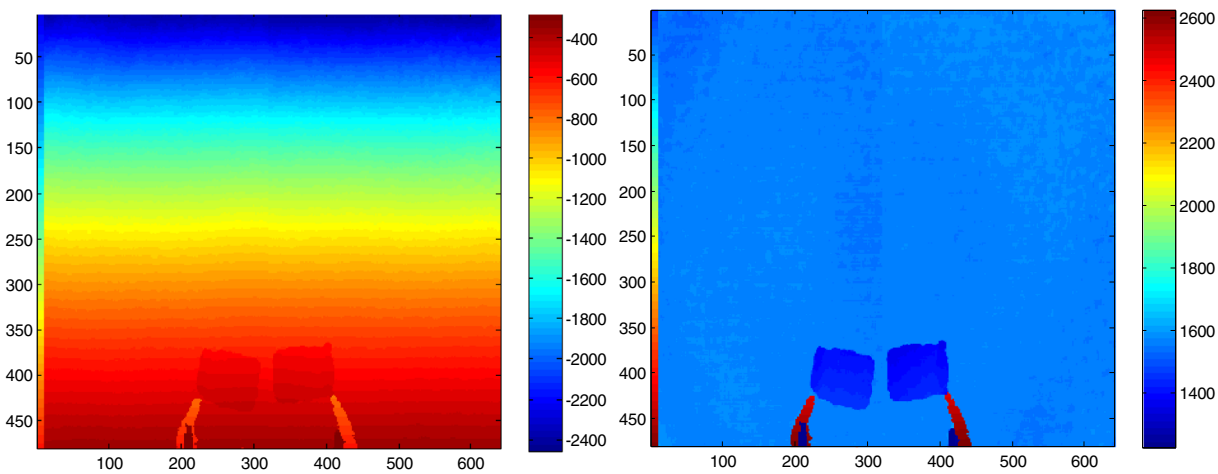

Fig. 5 The original (left) and corrected (right) depth map

Fig. 6 Background image and morphological operations applied image

forward by making a fist, hand release and waving the hand right, respectively. The user waves his hand left to stop the wheelchair. The classification accuracies for the making a fist and hand release tasks are observed to be higher compared to other tasks. Therefore, these tasks are selected for steering the wheelchair to the left and right. Three pre-defined tasks are used in EEG based control. The wheelchair is steered to left, right and forward through accomplishing the relaxing, math problem solving and text reading tasks, respectively. The wheelchair is stopped when continuous head movement is detected. An open loop control is applied on the wheelchair due to lack of encoders.

In the first phase of this study, EMG and EEG data was recorded and classified offline in MATLAB environment. Parameters of classifiers were determined using the trial and error method based on the offline data analysis. Two seconds of EMG data was recorded from each subject while accomplishing the pre-defined four tasks. For the EEG case, ten seconds of data was recorded from each subject while accomplishing the pre-defined three cognitive tasks. Ten trials were conducted for each EMG and EEG task.

In the offline data processing the EEG signals were divided into one second time windows. Head movements can affect the EEG data and are usually referred to as artifacts. EEG data windows containing head movement artifacts were detected and discarded through gyro data analysis based elimination method. The mean value of the first order derivative of gyro data in time domain (GYROX and GYROY) was calculated for each window. Gyro data windows, which had a mean value lower than a certain threshold, were regarded as artifact free data. The remaining windows were discarded and not used for the task classification. In the real time experiments, continuous head movements were used to stop the wheelchair. Sample EEG data in AF3, gyro data and artifact detection results are given in Fig. 7.

5.0.1 Feature extraction

In feature extraction the input signal is transformed into a new smaller space of variables that simplifies analysis [27]. Time domain based features are frequently used for EMG signal classification since time domain features can be implemented and computed easily [28]. In addition to time domain features, frequency domain and wavelet transform based features are utilized for EMG signal classification [29]. In this study, time domain features were used in order to define EMG movements. The features used in this study consisted of mean absolute value, standard deviation, number of zero crossing, line-length and approximate entropy. The line-length quantifies the predictability of a signal and can be calculated as follows,

$$L = \sum_{j=1}^{N} \left| x_{j+1} - x_j \right| \tag{21}$$

In the literature, EEG band energies are commonly used for EEG signal classification applications. In this study energies contained in theta, alpha and beta bands were included in the feature vector for EEG signal classification. The features used in bio-signal classification are summarized in Table 2. The EMG feature vector consists of 40 elements extracted from 8 channels and the EEG feature vector consists of 98 elements extracted from 14 channels.

5.0.2 Bio-Signal Classification

Combination of classifiers is often used in the literature to improve classification performance in complex

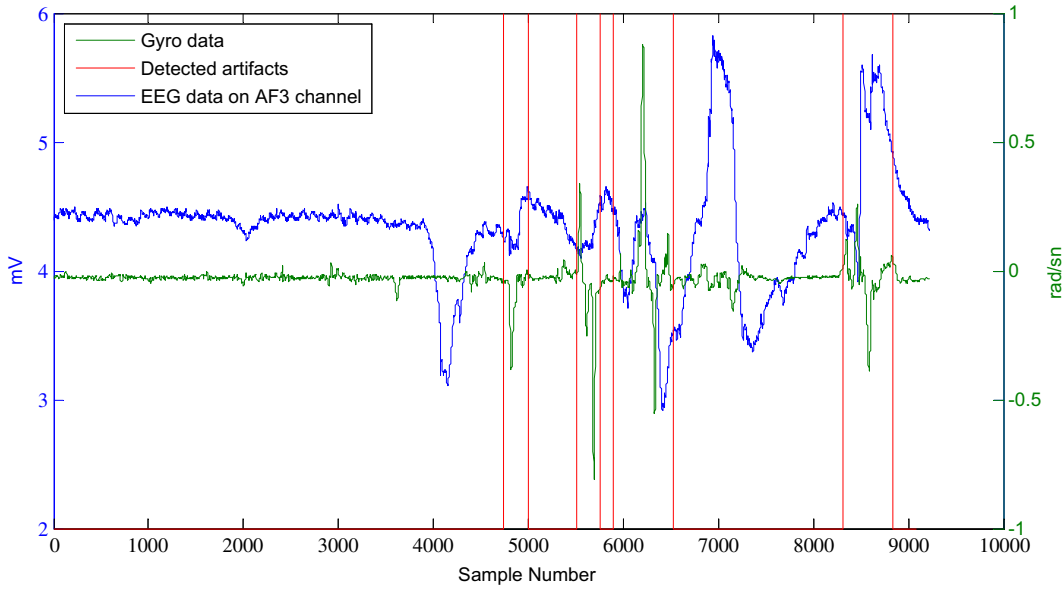

Fig. 7 EEG, GYRO data and detected artifacts

problems [30]. In this study, classification is performed based on the combined decisions of ANN, SVM and random forest classifiers.

As mentioned in the previous section, two seconds of EMG data were acquired during each task. Ten trials were conducted by four subjects for each task. The EMG data was segmented into 50 ms time windows resulting in a dataset of 1600 epochs for each task. For EEG based classification, 10 seconds of EEG data were acquired for each cognitive task. Ten trials were conducted by three subjects for each task. The EEG data was segmented into 1 second time windows resulting in a dataset of 300 epochs for each task. Randomly selected 70 % of the dataset was used for training the classifiers while the remaining 30 % was used for testing the classifiers' performance.

Table 2 Selected features for bio-signal classification

Feature	EEG classification	EMG classification
Mean absolute value	√	√
Standard deviation	√	√
Line Length	√	√
Number of zero cross		√
Ap-En	√	√
Band energies (theta, alpha and beta)	√	

For the ANN based classifier, the number of hidden layers and neurons were set to 2 and 40 (for each hidden layer), respectively. The classifier was trained with the back-propagation algorithm. Tansig function was selected as the activation function of the neural network. For the random forest tree classifier, the number of trees was set to. The parameters of all three classifiers were determined by trial and error method during offline data analysis.

In the training phase, for each subject, each classifier was trained with features extracted from the training data set. The signal class was decided according to most voted task. Since SVM classifiers can only separate two different classes with one model, two different strategies are used in multiclass classification. Building a one versus all SVM classifier model for each class is a commonly used strategy in practice. Building a set of one versus one SVM models is another strategy used in literature. In this study, one versus all strategy was adopted in SVM based signal classification. In bio-signal data processing, the classification result of the ANN classifier was assumed to be valid if the absolute difference between the actual output and any of the desired outputs is less than a threshold. If the ANN model outputs a valid result, the classification is performed based on the majority of vote. Otherwise the proposed algorithm checks the results of the SVM and RF classifiers. If both

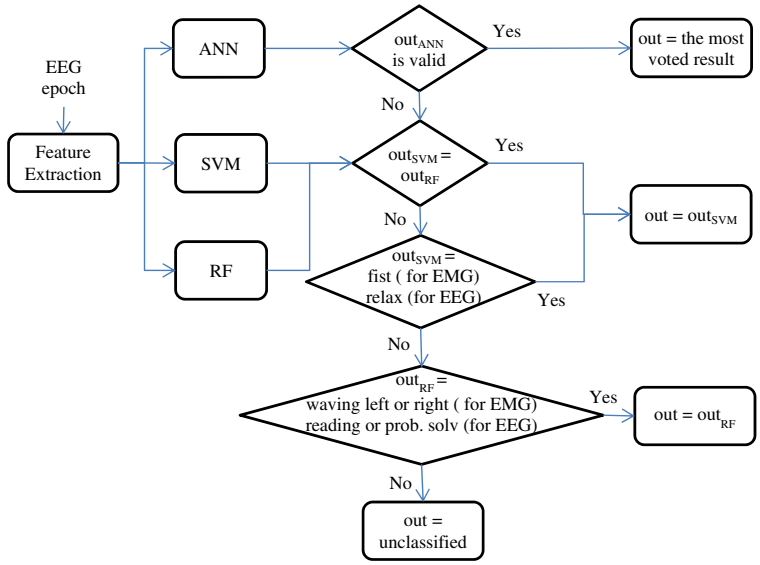

Fig. 8 Flow-chart for the proposed rule-based scheme

classifiers agree on a class, the proposed algorithm accepts the decision. If this is not the case, the classification result of the SVM is checked. If the SVM classifies EMG data into fist class, the data is classified as fist. This decision is based on the fact that the performance of the SVM classifier is much better than the RF classifier for the related class. Similarly, if the SVM classifies EEG the data into relax class, the data is classified as relax. If the data is still not classified, the output of the RF classifier is checked. In case the output is waving-left or waving right for the EMG data, the algorithm's final decision agrees with the RF classifier. Similarly, in case the output of the RF classifier is text reading or math problem solving for the EEG data, the algorithm's final decision agrees with the RF classifier. Data that is not classified at this stage is assumed to be unclassified. The flow-chart of the developed algorithm is given in Fig. 8.

Table 3 Confusion table and the sensitivity values for EMG classifiers

Predicted actual	Classifier	Fist	Release	Left	Right	Un-classified
Fist	ANN	220 (.458)	130	79	20	31
	SVM	407 (.848)	1	25	34	13
	RF	385 (.802)	0	44	51	0
	Proposed	408 (.850)	1	20	25	26
Release	ANN	0	474 (.988)	6	0	0
	SVM	3	472 (.983)	2	2	1
	RF	0	478 (.996)	2	0	0
	Proposed	0	479 (.998)	1	0	0
Waving left	ANN	11	122	328 (.683)	19	0
	SVM	82	2	335 (.698)	10	51
	RF	51	0	400 (.833)	29	t0
	Proposed	28	2	405 (.844)	37	8
Waving Right	ANN	8	48	141	282 (.588)	1
	SVM	85	3	32	323 (.673)	37
	RF	41	0	37	402 (.838)	0
	Proposed	28	1	35	407 (.848)	9

Table 4 Specificity values for the EMG based classifiers

	Fist	Release	Left	Right	Average
ANN	0.987	0.689	0.797	0.966	0.860
SVM	0.882	0.994	0.947	0.959	0.945
RF	0.936	1	0.920	0.923	0.945
Proposed	0.961	0.996	0.946	0.940	0.961

6 Results and Discussion

The performance of the proposed system was evaluated in two different ways. First, bio-signal data acquired from four different subjects were processed offline in MATLAB environment. The data was classified using ANN, SVM, random forest and the proposed schemes. The performance of the classifiers was evaluated based on sensitivity and specificity defined by,

$$Sensitivity = \frac{TP}{(TP + FN)} \tag{22}$$

$$Specifity = \frac{TN}{(TN + FP)} \tag{23}$$

TP, TN, FP and FN stands for true positives, true negatives, false positives and false negatives, respectively. True positives are the correctly classified data samples in a related class whereas true negatives are the correctly classified data samples belonging to other classes. False negatives are the data samples in a class incorrectly classified as belonging to one of the other classes. False positives on the other hand are the data samples in other classes incorrectly classified as the class of interest.

The developed wheelchair system was also tested in real-time by four different subjects. The subjects were asked to track a sinusoidal route drawn on a floor by controlling their EMG and EEG activity.

6.1 Offline Classification Results

Offline EMG classification results for the four predefined tasks are provided in Table 3. The table illustrates the confusion table and the classifier sensitivities for the ANN, SVM, RF and the proposed classifiers. The rows and columns in the table represent the actual and the predicted classes, respectively. Results provided are the totals for all subjects. It was observed that all classifiers including the proposed scheme showed better performance in classifying fist and hand release tasks. This is expected since EMG signals become noticeably strong for all 8 channels when a subject makes a fist. Similarly, EMG signals become noticeably weak for all 8 channels when a subject releases his hand. The SVM classification accuracy for the making fist task was higher than that of the other classifiers' accuracies. On the other hand, the RF classifier has a better performance in

Table 5 Confusion table and the sensitivity values for EEG classifiers

	Classifier	Relax	Text reading	Math problem solving	Un-classified
Relax	ANN	43 (.478)	40	4	3
	SVM	75 (.833)	7	6	2
	RF	72 (.800)	10	8	0
	Proposed	81 (.900)	0	0	9
Text reading	ANN	0	69 (.767)	12	9
	SVM	0	65 (.722)	7	18
	RF	2	73 (.811)	15	0
	Proposed	5	74 (.822)	11	0
Math problem solving	ANN	3	20	64 (.711)	3
	SVM	0	15	65 (.722)	10
	RF	6	15	69 (.767)	0
	Proposed	0	14	76 (.844)	0

Table 6 Specificity values for the EEG based classifiers

	Relax	Text reading	Math problem solving	Average
ANN	0.978	0.459	0.862	0.767
SVM	1	0.809	0.887	0.899
RF	0.926	0.766	0.793	0.828
Proposed	0.950	0.868	0.894	0.904

classifying the remaining three hand movements. The proposed method as discussed earlier makes a decision based on rules constructed on the individual outputs of the ANN, SVM and RF classifiers.

Out of the 480 EMG test epochs corresponding to fist, 408 (sensitivity: 0.85) were correctly classified by the proposed scheme. The classifier sensitivities for the release, waving left and waving right were 0.998, 0.844 and 0.848, respectively. The classifier sensitivities over all classes were 0.679, 0.801, 0.867 and 0.885 for the ANN, SVM, RF and proposed scheme, respectively. The unclassified data was included in false negatives when computing the sensitivities. The proposed method's misclassification percentage, discarding the unclassified data, was 9.3 % as compared to 30.4 %, 14.6 % and 13.3 % misclassification rates for the ANN, SVM and RF classifiers. Results confirm that the proposed method outperforms all three classifiers.

Table 4 depicts the specificity values computed for the EMG based classifiers. The average specificities of ANN, SVM, RF and the proposed classifiers were 0.860, 0.945, 0.945 and 0.961, respectively. Having the highest average specificity, the proposed classifier outperformed the other classifiers.

Offline EEG classification results for the three pre-defined tasks are provided in Table 5. The table illustrates the confusion table for the ANN, SVM, RF and the proposed classifiers. The rows and columns in the table represent the actual and the predicted classes, respectively. Results provided are the totals for all subjects. The SVM classification sensitivity for the relaxing cognitive task is higher than that of the other classifiers' sensitivities. The RF classifier on the other hand has a better performance in classifying text reading and math problem solving tasks. Out of the 90 epochs corresponding to relaxing class, 81 (sensitivity: 0.90) were correctly classified by the proposed scheme. The classification sensitivities for the text reading and math problem solving were 0.822 and 0.844, respectively. The classifier sensitivities over all classes were 0.651, 0.759, 0.792 and 0.855 for the ANN, SVM, RF and proposed scheme, respectively. The proposed method's misclassification percentage was 11.11 % as compared to 30.7 %, 12.9 % and 20.7 % misclassification rates for the ANN, SVM and RF classifiers. Similar to the results for EMG based control, the proposed method outperforms all three classifiers.

Table 6 depicts the specificity values computed for the EEG based classifiers. The average specificities of ANN, SVM, RF and the proposed classifiers were 0.767, 0.899, 0.828 and 0.904, respectively. Besides having the highest sensitivity, the proposed scheme also had the highest specificity.

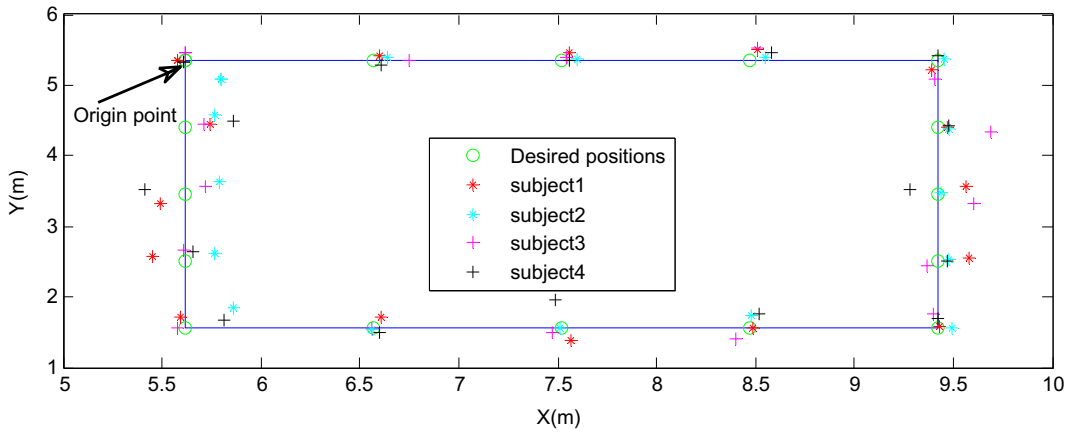

Fig. 9 Rectangular route results for EMG based control

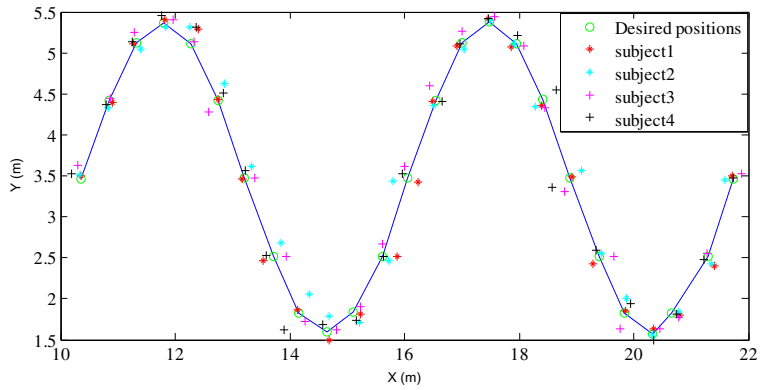

Fig. 10 Sinusoidal route results for EMG based control

6.2 Real-time Performance Results

Three benchmark routes were used to observe the real-time system performance of EMG based control of the developed wheelchair. The subjects were asked to track a rectangular, sinusoidal and an elliptic route by controlling the robotic wheelchair through accomplishing the related tasks. During the experiments, the wheelchair was stopped at regular intervals and exact position measurements were taken with a laser sensor. Position measurements were performed with respect to the center point of the wheelchair. The route tracking performance of the four subjects for the rectangular route is provided in Fig. 9. Turning with zero radius to left and in counter clockwise is the challenging movement in the rectangular route. As it is clearly seen from the figure, position errors increased during the 90 degree turns at the corners. It is challenging to keep the wheelchair on the route right after the wheelchair turns the corners. The obvious difference between the tracking performances of the subjects is highly related to the experience level. The stopping of the wheelchair at regular intervals to take position measurements negatively affected the subjects' performances and increased position errors.

The route tracking performance of the subjects for the sinusoidal route is provided in Fig. 10. Turning at the local extreme points is the challenging movement in the sinusoidal route. As it is clearly seen from the figure, position errors increase when the wheelchair turns these points at which there is a sharp change in the route's direction. Subjects should make an immediate turn at the related points to keep wheelchair on the route.

The route tracking performance of the subjects for the elliptic route is provided in Fig. 11. In the elliptic route, subjects should turn continuously to keep the wheelchair on the route. The subjects tracked the

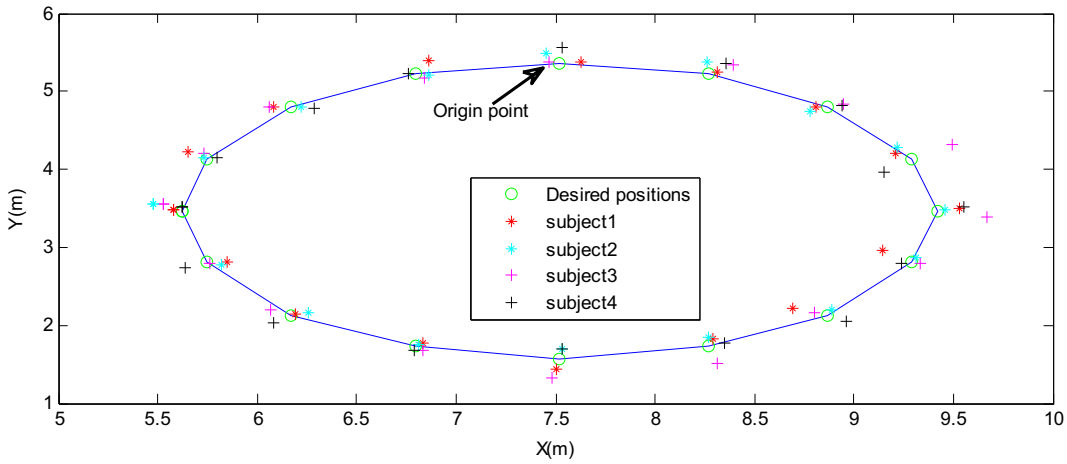

Fig. 11 Elliptic route results for EMG based control

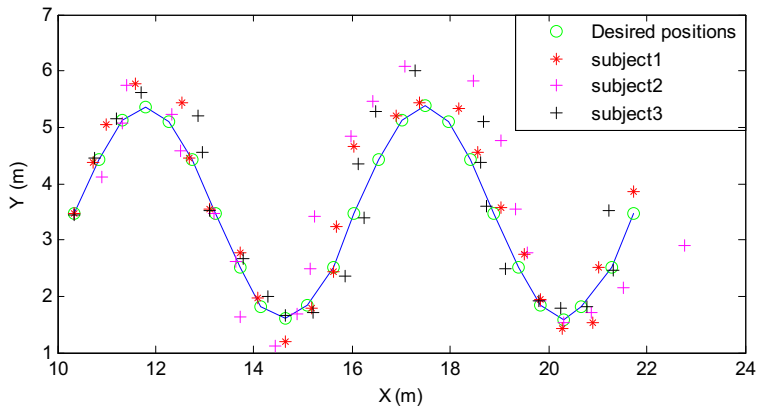

Fig. 12 Sinusoidal route results for EEG based control

elliptic route in clockwise manner. Compared to the other routes, subjects were challenged at every single point of the route.

The performance of the EMG based control of robotic wheelchair system was observed to be affected by fatigue. Fatigue time varied between 45 minutes and one hour among subjects. On the other hand, EEG based control was not robust against environmental effects which caused distraction. Thus, EEG based experiments were performed in a controlled environment. During the experiments, a transition period was observed during task switching. Therefore, the user command was assumed to be valid only if the algorithm evaluated to same result for the two consecutive EEG epochs. Once a valid command was detected, the wheelchair was then navigated through corresponding direction; otherwise the wheelchair was stopped. Thus, at least two seconds was required to send a new command through EEG. Consequently, it was very challenging to keep the wheelchair on the route through EEG control for the paths that frequently change direction and require high degrees of maneuverability. Therefore, only sinusoidal route was tracked in EEG based control of the wheelchair. The route tracking performance of the three subjects for the sinusoidal route is provided in Fig. 12.

Root mean square (RMS) of position errors between desired positions ($\mathbf{x}^{\text{desired}}$) and actual positions ($\mathbf{x}^{\text{actual}}$) were calculated based on the following equation.

$$e_{RMSE} = \sqrt{\frac{\sum_{n=1}^{N} \left(x_n^{desired} - x_n^{actual}\right)^2}{N}} \tag{24}$$

EMG route tracking performances for the four subjects is illustrated in Table 7. RMS of position errors for the rectangular, sinusoidal and the elliptic route for the most experienced user (subject 1) were 0.1294m, 0.1154m and 0.1154m, respectively. The performances of the other users were slightly worse as compared to subject 1.

EEG route tracking performances for the three subjects is illustrated in Table 8. RMS of position errors for the sinusoidal route were 0.2804m, 0.5180m and 0.3258m for the three subjects. The RMS of errors for EEG experiments was observed to be higher as compared to the ones computed for the EMG case. This was expected since controlling brain signals is

Table 7 EMG based control route tracking errors

	Rectangular route (in meters)	Sinusoidal route (in meters)	Elliptic route (in meters)
Subject 1	0.1294	0.1154	0.1154
Subject 2	0.1816	0.1546	0.1088
Subject 3	0.1585	0.1607	0.1473
Subject 4	0.1654	0.1468	0.1187

Table 8 EEG based control route tracking errors

	Sinusoidal route (in meters)
Subject 1	0.2804
Subject 3	0.5180
Subject 4	0.3258

more challenging than controlling muscles. In addition, users performing EEG tasks were more easily distracted by external disturbances. As mentioned earlier, the stopping of the wheelchair at regular intervals to take position measurements also negatively affected the subjects' performances and increased position errors. The subjects were observed to perform considerably better when the wheelchair was not stopped for position measurements.

7 Conclusions and Future Work

In this study, EMG and EEG based control of a robotic wheelchair was proposed. Safe navigation of the developed system was provided through processing depth images acquired from widely available and low-cost Kinect sensor. In addition to Kinect sensor, LIDAR and ultrasonic sensors can be installed on the wheelchair system to improve safety. An open loop control was applied on motors since encoders could not be mounted on the motors due to mechanical constraints.

Thalmic Labs wearable low-cost arm-band was used for real time EMG data collection. The performance of EMG based control of the system was satisfactory. The armband can be used in EMG based control of real time systems instead of expensive professional EMG devices. Emotive EEG headset was used in real time EEG data collection. Robotic wheelchair was controlled by processing two seconds EEG windows. Due to resulting delay, the cruise speed of the robotic wheelchair system was limited to 20 cm/s. The cruise speed was set to 60 cm/s for the EMG based control since shorter windows were required for task classification. To improve the EEG based control performance of the robotic wheelchair system, a professional EEG system should be used.

In addition to bio-signal based control, a vision based eye ball tracking system will be developed and installed on the system.

References

1. Boquete, L., Garcia, R., Barea, R., Mazo, M.: Neural control of the movements of a wheelchair. Int. J. Intell. Robot. Syst. **25**, 213–226 (1999)
2. Barea, R., Boquete, L., Mazo, M., Lopez, E.: Wheelchair guidance strategies using EOG. Int. J. Intell. Robot. Syst. **34**, 279–299 (2002)
3. Jeonghee, K., Hangue, P., Joy, B., Erica, S., Diane, R., Deborah, P., Jaimee, H., Julia, M., Beatrice, N., Dennis, W., Anne, L., Eliot, R., Mike, J., Emir, V., Maysam, G.: The tongue enables computer and wheelchair control for people with spinal cord injury. Sci. Trans. Med. **5**(1), 166–213 (2013)
4. Carlson, T., Millan, J.R.: Brain-controlled wheelchairs: A robotic architecture. IEEE Robot. Autom. Mag. **20**(1), 65–73 (2013)
5. Kim, K.H., Kim, H.K., Kim, J.S., Wookho, S., Lee, S.D.: An EMG-based human interface for the control of an electrically powered wheelchair. Int. J. Robot. Autom **28**(1), 111–114 (2006)
6. Grasse, R., Morere, Y., Pruski, A.: Assisted navigation for persons with reduced mobility: path recognition through particle filtering (condensation algorithm). Int. J. Intell. Robot. Syst. **60**, 19–57 (2010)
7. Yoshiyuki, N., Akira, K., Kazuhiko, T.: A mechatronics vision for smart wheelchairs. Int. J. Robot. Autom. **30**(1), 611–627 (2008)
8. Gulrez, T., Tognetti, A.: A sensorized garment controlled virtual robotic wheelchair. Int. J. Intell. Robot. Syst. **74**, 847–868 (2014)
9. Zhenghui, G., Zhuliang, Y., Zhifang, S.: An online semi-supervised brain–computer interface. IEEE Trans. Biomed. Eng. **8**, 2614–2623 (2013)
10. Christopher, B., Alric, A., Paul, D.G.: A Brain?Computer Interface (BCI) for the detection of mine-like objects in sidescan sonar imagery. IEEE J. Ocean. Eng. **41**, 123–138 (2016)
11. Riccardo, B., Francesco, B., Alessandro, D.G., Danu, P., Carlotta, S.: Electroencephalogram and physiological signal analysis for assessing flow in games. IEEE Trans. Comput. Intell. AI in Games **5**, 164–175 (2013)
12. Konstantin, P.G., Petr, K.G., Mikhail, I.S.: Stable sequential Kuhn-Tucker theorem in one-dimensional inverse problems of dielectric reflectometry. Proc. 8th IEEE Int. Conf. Commun. Syst. Netw. (COMSNETS) **2**, 1–4 (2015)
13. Novi, Q., Zoubin, G.: very simple safe-bayesian random forest, A, IEEE Trans. Pattern Anal. Mach. Intell, 37, 6,1297–1303 (2015)
14. Scornet E.: Random forests and kernel methods. IEEE Trans Inf. Theory **62**(3), 1485–1500 (2016)
15. Ocak, H.: Automatic detection of epileptic seizures in EEG using discrete wavelet transform and approximate entropy. Expert Syst. Appl. **36**(2), 2027–2036 (2009)
16. Sathiyanarayanan M.: MYO Armband for physiotherapy healthcare: A case study using gesture recognition application, Proceedings of the 16th IEEE International Conference on Transparent Optical Networks (ICTON), 1–6 (2016)
17. Luh, G.C., Lin, H.A., Ma, Y.S., Yen, C.J.: Intuitive muscle-gesture based robot navigation control using wearable

gesture armband, Proceedings of the IEEE International Conference on Machine Learning and Cybernetics (ICMLC), 389–395 (2015)
18. Gundlapalli, V.S.K., Shaik, Y.F., Muhammad, Z.U.R., Shaik, R.A., Aimé, L.E.: Efficient signal conditioning techniques for brain activity in remote health monitoring network. IEEE Sens. J. **13**(9), 3276–3283 (2013)
19. Zhendong, L., Shun, H., Feng, D.: The development of a smart house system based on Brain-Computer Interface, Proceedings of the IEEE International Conference on Robotics and Biomimetics (ROBIO), 1012–1017 (2015)
20. Shouyi, W., Jacek, G., Chaovalitwongse, W.A.: Using wireless EEG signals to assess memory workload in the n-back task. IEEE Trans. Human-Mach. Syst. **46**(3), 424–434 (2016)
21. Raul, C.C., Edmundo, B.H., Federico, R.C., Roberto, M.C., Carlos, P.C.: Facial expression analysis with kinect for the diagnosis of paralysis using nottingham grading system. IEEE Latin Am. Trans. **14**(12), 3418–3426 (2016)
22. Enrico, B., Pietro, P., Stefano, B., Alberto, D.B.: Sequences, reconstructing high-resolution face models from kinect depth. IEEE Trans. Inf. Forensic. Secur. **11**(12), 2843–2853 (2016)
23. Seokmin, H., Adrian, D., Genaro, S., Juan, C.B., Manuel, M.C.: Three-dimensional integral-imaging display from calibrated and depth-hole filtered kinect information. J. Disp. Technol. **12**(11), 1301–1308 (2016)
24. Zhao, Z., Liu, Y., Zhang, Z.: Camera calibration with three noncollinear points under special motions. IEEE Trans. Image Process. **17**(12), 2393–2402 (2008)
25. Rahman, T., Krouglicof, N.: An efficient camera calibration technique offering robustness and accuracy over a wide range of lens distortion. IEEE Trans. Image Process. **21**(2), 626–637 (2012)
26. Tzung-Sz, S., Chia-Hsiang, M.: Automatic camera calibration for a multiple-sensor integrated coordinate measurement system. IEEE Trans. Robot. Autom. **17**(4), 502–507 (2001)
27. Robert, J., Angelika, P., Martin, B.: Feature extraction and selection for emotion recognition from EEG. IEEE Trans. Affect. Comput. **5**(3), 327–339 (2014)
28. Matsubara, T., Morimoto, J.: Bilinear modeling of EMG signals to extract user-independent features for multiuser myoelectric interface. IEEE Trans. Biomed. Eng. **60**(8), 2205–2213 (2013)
29. Mahaphonchaikul, K., Sueaseenak, D., Pintavirooj, C., Sangworasil, M., Tungjitkusolmun, S.: EMG signal feature extraction based on wavelet transform, Proceedings of the 20th IEEE International Conference on Electrical Engineering/Electronics Computer Telecommunications and Information Technology (ECTI-CON), 327–331 (2010)
30. Xie B., Minn H.: Real-time sleep apnea detection by classifier combination. IEEE Trans. Inf. Technol. Biomed. **16**(3), 469-477 (2012)

Gurkan Kucukyildiz received his B.S and M.S. degrees from Kocaeli University, Kocaeli, Turkey in 2009 and 2012, in Communication and Electronics Engineering and Mechatronics Engineering, respectively. He is currently a research assistant at Mechatronics Engineering Department at Kocaeli University. His research interests include pattern recognition, biomedical signal processing, computer vision and embedded systems.

Hasan Ocak received his B.S., M.S. and Ph.D. degrees from Case Western Reserve University, Cleveland, OH, USA in 1997, 1999 and 2004, respectively, all in Electrical Engineering. He is a Full Professor of Mechatronics Engineering Department at Kocaeli University, Kocaeli, Turkey. Dr. OCAK is currently the department chair and the coordinator for the Machine Vision Laboratory. His research interests include pattern recognition, biomedical signal processing, computer vision and intelligent systems.

Suat Karakaya is a research assistant at Kocaeli University, Turkey. He received his B.S. degree in Mechatronics Engineering from Kocaeli University in 2011. Then, he joined the Machine Vision Laboratory of Mechatronics Engineering Department in Kocaeli University. In 2014, he participated as an intern researcher in an R&D project supported by The Scientific and Technological Research Council of Turkey (TUBITAK) under the grant number TUBITAK-113E777. His research areas include mobile robotics, collision avoidance and control theory.

Omer Sayli received his B.S. and M.S degrees in Electrical and Electronics Engineering from Bogazici University, Istanbul, Turkey. In 2009, he received his Ph.D. degree from Bogazici University in Biomedical Engineering. Dr. Sayli's active research focuses on signal processing for biomedical applications.